Synthesis of Poly(2-oxazoline)s with Side Chain Methyl Ester Functionalities: Detailed Understanding of Living Copolymerization Behavior of Methyl Ester Containing Monomers with 2-Alkyl-2-oxazolines

Petra J. M. Bouten,[1,2] Dietmar Hertsen,[3] Maarten Vergaelen,[1] Bryn D. Monnery,[1] Saron Catak,[3,4] Jan C. M. van Hest,[2] Veronique Van Speybroeck,[3] Richard Hoogenboom[1]

[1]Supramolecular Chemistry Group, Department of Organic and Macromolecular Chemistry, Ghent University, Krijgslaan 281 S4, 9000 Ghent, Belgium

[2]Radboud University Nijmegen, Institute for Molecules and Materials (IMM), Heijendaalseweg 135, 6525 AJ Nijmegen, The Netherlands

[3]Center for Molecular Modeling (CMM), Ghent University, Technologiepark 903, Zwijnaarde 9052, 9000 Ghent, Belgium (Member of the QCMM Ghent–Brussels Alliance)

[4]Department of Chemistry, Bogazici University, Bebek, 34342 Istanbul, Turkey

Correspondence to: V. Van Speybroeck (E-mail: veronique.vanspeybroeck@ugent.be) or R. Hoogenboom (E-mail: richard.hoogenboom@ugent.be)

Received 9 April 2015; accepted 3 June 2015; published online 00 Month 2015
DOI: 10.1002/pola.27733

ABSTRACT: Poly(2-oxazoline)s with methyl ester functionalized side chains are interesting as they can undergo a direct amidation reaction or can be hydrolyzed to the carboxylic acid, making them versatile functional polymers for conjugation. In this work, detailed studies on the homo- and copolymerization kinetics of two methyl ester functionalized 2-oxazoline monomers with 2-methyl-2-oxazoline, 2-ethyl-2-oxazoline, and 2-*n*-propyl-2-oxazoline are reported. The homopolymerization of the methyl ester functionalized monomers is found to be faster compared to the alkyl monomers, while copolymerization unexpectedly reveals that the methyl ester containing monomers significantly accelerate the polymerization. A computational study confirms that methyl ester groups increase the electrophilicity of the living chain end, even if they are not directly attached to the terminal residue. Moreover, the electrophilicity of the living chain end is found to be more important than the nucleophilicity of the monomer in determining the rate of propagation. However, the monomer nucleophilicity can be correlated with the different rates of incorporation when two monomers compete for the same chain end, that is, in copolymerizations. © 2015 Wiley Periodicals, Inc. J. Polym. Sci., Part A: Polym. Chem. **2015**, *00*, 000–000

KEYWORDS: copolymers; density functional theory; molecular dynamics; molecular modeling; polymerization kinetics; poly(2-oxazoline)s

INTRODUCTION The living cationic ring-opening polymerization (CROP) of 2-oxazoline monomers (Scheme 1) was first reported in the 1960s[1–4] providing an easy access to a wide variety of well-defined poly(2-alkyl/aryl-2-oxazoline)s (PAOx) with controlled end-group functionality during initiation and termination.[5–9] PAOx are an interesting class of polymers because of its highly tunable and diverse properties.[6,10–12] Poly(2-methyl-2-oxazoline) (PMeOx) and poly(2-ethyl-2-oxazoline) (PEtOx) are of special interest for biomedical applications because of their biocompatibility and stealth behavior that are similar to poly(ethylene glycol) (PEG).[6,10,11,13] PEtOx and poly(2-propyl-2-oxazoline) (PProOx) show lower critical solution (LCST) behavior with better reversibility as compared to the gold standard poly(*N*-isopropylacrylamide).[14–16] The properties of PAOx can be easily tuned by variation of the side chain substituent, also enabling the incorporation of (protected) side chain functionalities.[17–30]

PAOx with methyl ester functionalized side chains are especially interesting as the methyl ester can be hydrolyzed to the carboxylic acid, a versatile functionality for conjugation of peptides and proteins. Furthermore, the methyl ester group can undergo a direct noncatalyzed amidation reaction to easily introduce a wide variety of side chain amide moieties.[31,32] Very recently, we reported an increased

Petra J. M. Bouten and Dietmar Hertsen contributed equally to this work.

Additional Supporting Information may be found in the online version of this article.

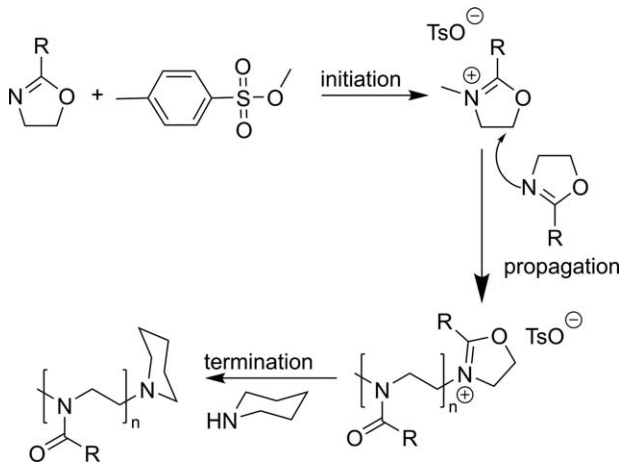

SCHEME 1 Cationic ring-opening polymerization of 2-oxazolines with methyl *p*-toluenesulfonate as initiator and piperidine as terminating agent.

propagation rate of the methyl ester containing monomer 2-methoxycarbonylethyl-2-oxazoline (MestOx, **1**) (Scheme 2) during homopolymerization compared to 2-methyl-2-oxazoline (MeOx, **3**) or 2-ethyl-2-oxazoline (EtOx, **4**), while copolymerization surprisingly revealed slower incorporation of MestOx.[28] Previous computational modeling suggested that the methyl ester group of the MestOx interacts with the living chain end, causing a slight increase in electrophilicity of the carbon atom C5, thereby enhancing the reactivity of the oxazolinium ring. The nitrogen atom of the MeOx monomer is more negative, and thus more nucleophilic and reactive towards the chain end, than the nitrogen atom of the MestOx monomer. This theory is indirectly supported by the work of Saegusa and Ikeda.[33] Nearby ester groups in the growing polymer can also interact with the incoming MeOx monomer, inducing higher nucleophilicity of the MeOx monomer.

In this contribution we describe the synthesis of a new methyl ester containing monomer with a trimethylene (C3) spacer between the oxazoline ring and the methyl ester namely 2-methoxycarbonylpropyl-2-oxazoline (C3MestOx, **2**). Detailed studies on the homo- and copolymerization kinetics of these two methyl ester functionalized 2-oxazoline monomers, MestOx and C3MestOx, with MeOx, EtOx, and 2-*n*-propyl-2-oxazoline (nPropOx, **5**) are reported. To better understand the observed copolymerization rate constants, the Arrhenius parameters of MestOx, C3MestOx, and MestOx–MeOx copolymerization were also determined by studying the (co)polymerization at different temperatures. Theoretical calculations were performed to compare the

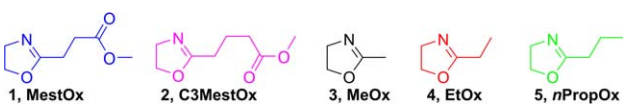

SCHEME 2 Monomer structures of MestOx (**1**), C3MestOx (**2**), MeOx (**3**), EtOx (**4**), and nPropOx (**5**). [Color figure can be viewed in the online issue, which is available at wileyonlinelibrary.com.]

nucleophilicities of the monomers and to assess the effect of the methyl ester side chains in MestOx and C3MestOx on the electrophilicity of the living cationic center. The computational approach consists of static density functional theory (DFT) calculations on monomers, cationic chains and propagation systems, as well as a semiempirical molecular dynamics trajectory of a MestOx decamer, whereby the time evolution of interactions is observed.

EXPERIMENTAL

Materials

2-Chloroethylamine hydrochloride, methyl *p*-toluenesulfonate (MeOTs), and sodium carbonate were purchased from Acros Organics. EtOx was kindly donated by Polymer Chemistry Innovations. All other reagents were purchased from Sigma Aldrich and used as received, except MeOx, EtOx, and MeOTs. These were purified by distillation over barium oxide and stored under argon. Dry solvents were obtained from a solvent purification system from J. C. Meyer, with aluminum oxide drying system and a nitrogen flow.

Instrumentation

Nuclear magnetic resonance (NMR) spectra were recorded on a Bruker DMC300 (300 MHz for ^{1}H, 75 MHz for 13C) or a Bruker DMX 500 (500 MHz for ^{1}H, 125 MHz for 13C).

Electro spray ionization mass (ESI MS) spectra were recorded on a Thermo Finnigan LCQ Advantage Max.

HR-MS was measured on an Agilent 1100 series HPLC coupled to an Agilent 6220A TOF-MS equipped with ESI/APCI multimode source.

Polymerization reaction mixtures were prepared in a VIGOR Sci-Lab SG 1200/750 Glovebox system, with less than 1 ppm of O_2 and H_2O.

Polymerizations were conducted in a Biotage Initiator Microwave System with Robot Sixty utilizing capped reaction vials. These vials were heated to 120 °C overnight, allowed to cool to room temperature and filled with nitrogen prior to use. All microwave polymerizations were performed with temperature control (IR sensor).

Size exclusion chromatography (SEC) was performed on an Agilent 1260—series HPLC system equipped with a 1260 ISO-pump, a 1260 automatic liquid sampler, a thermostatted column compartment, a 1260 diode array detector (DAD), and a 1260 refractive index detector (RID). Analyses were performed on Mixed D columns and a guard column in series at 50 °C. *N,N*-dimethylacetamide (DMA), containing 50 mM of LiCl, was used as an eluent, at a flow rate of 0.593 mL min^{-1}. The SEC eluograms were analyzed using the Agilent Chemstation software with the GPC add on, calibrated against poly(methyl methacrylate) (PMMA) standards.

Gas chromatography (GC) was performed on a 7890A from Agilent Technologies with an Agilent J&W Advanced Capillary GC Column (30 m, 0.320 mm, and 0.25 μm). Injections were

performed with an Agilent Technologies 7693 auto sampler. Detection was done with a Flame ionization detector (FID) detector. Injector and detector temperatures were kept constant at 250 and 280 °C, respectively. The column was initially set at 50 °C, followed by two heating stages: from 50 to 100 °C with a rate of 20 °C min^{-1} and from 100 to 300 °C with a rate of 40 °C min^{-1}, and then held at this temperature for 0.5 min. Conversion was determined based on the integration of monomer peaks using acetonitrile (CH_3CN) as an internal standard.

Monomer Synthesis

Synthesis of Methyl 4-(2-chloroethyl)amino-4-oxobutanoate (1b, MestOx-precursor)[28]

Methyl succinyl chloride (**1a**, 100 g, 664.2 mmol, 91.76 mL) and 2-chloroethylamine hydrochloride (77.04 g, 664.2 mmol) were suspended in dry dichloromethane (DCM, 750 mL) under an argon atmosphere. The reaction mixture was cooled continuously to 0 °C while triethylamine (TEA) (144.50 g, 1428 mmol, 198.4 mL) was added dropwise within 2 h. The reaction was allowed to warm to room temperature overnight, after full addition of the TEA. The mixture was washed with water (2 × 50 mL) and brine (1 × 50 mL). The organic phase was dried over Na_2SO_4 and the solvent was removed under reduced pressure. The resulting product was purified by filtration column chromatography (neutral Al_2O_3, DCM:MeOH (methanol, 99:1) yielding product **1b** as a yellow oil (107 g, 617.7 mmol, 83%).

^{1}H NMR ($CDCl_3$, 500 MHz): $\delta = 6.1$ (br, 1H, NH), 3.68 (t, 2.1 Hz, 2H, CH_2Cl), 3.61 (m, 5H, OCH_3 and $C\underline{H}_2CH_2Cl$), 2.68 (t, 7.0 Hz, 2 H, NC—$OC\underline{H}_2$), 2.52 (t, 7.0 Hz, 2H, $C\underline{H}_2COOCH_3$).

^{13}C NMR (75 MHz, CDCl3): $\delta = 172.9$ (C═ONH), 171.1 (C═OOCH3), 51.4 (OCH3), 43.5 (CH2CH2Cl), 40.8 (CH2Cl), 30.5 (CH3C═OCH2), 28.8 (CH3C═OCH2CH2).

ESI MS: *m/z*: calculated 193.05, found 194.1 and 196.1 [$M + H^+$], 216.1 and 218.1 [$M + Na^+$].

Synthesis of 2-methoxycarbonylethyl-2-oxazoline (1, MestOx)[28]

The MestOx precursor (**1b**, 107 g, 617.7 mmol) and anhydrous sodium carbonate (52.7 g, 497.3 mmol) were mixed. The reaction was performed for 48 h by mounting the flask at a rotary evaporator (40 °C, 50 mbar) to allow good mixing of the salt in the viscous mixture, thereby providing a larger surface area for evaporation of the released CO_2. Subsequently DCM was added, the reaction mixture was filtered and the solvent was removed under reduced pressure. The oil was distilled twice over barium oxide, under reduced pressure yielding a colorless liquid that crystallized in time into a white solid (60 g, 381.8 mmol, 69%).

^{1}H NMR ($CDCl_3$, 500 MHz,): $\delta = 4.3$ (t, 2H, 9.4 Hz, CH_2O), 3.8 (t, 9.4 Hz, 2H, CH_2N═), 3.7 (s, 3H, $COOCH_3$), 2.7 (t, 2H, 7.3 Hz, CH_2COO), 2.6 (t, 2H, 7.3 Hz, CH_2C(═N)O).

^{13}C NMR ($CDCl_3$, 75 MHz): $\delta = 172.9$ ($\underline{C}OOCH_3$), 169.2 (C(═N)O), 67.6 (CH_2O), 54.3 (CH_2N), 51.9 (OCH_3), 30.2 ($\underline{C}H_2COO$), 23.2 (CH_2N).

ESI MS: *m/z*: calculated 157.07, found 158.1 and 159.1 [$M + H^+$].

HR-MS: *m/z*: theoretical 157.07389 Da, found 158.0811 Da [$M + H^+$]; Δ abundance 0.4 ppm.

Synthesis of Methyl 5-(2-chloroethylamino)-5-oxopentanoate (2b, C3MestOx precursor)

Glutaric acid monomethyl ester chloride (**2a**, 50 g, 303.8 mmol, 41.98 mL) and 2-chloroethylamine hydrochloride (35.24 g, 303.8 mmol) were suspended in dry dichloromethane (375 mL) under an argon atmosphere. The reaction mixture was cooled continuously to 0 °C while triethylamine (66.09 g, 653 mmol, 90.8 mL) was added dropwise within 2 h. The reaction was allowed to warm to room temperature overnight, after full addition of the TEA. The mixture was washed with water (2 × 25 mL) and brine (1 × 25 mL). The organic phase was dried over Na_2SO_4 and the solvent was removed under reduced pressure. A yellow liquid (60 g, 289 mmol, 95%) was obtained.

^{1}H NMR (CDCl3, 300 MHz): $\delta = 6.0$ (br, 1H, NH), 3.67 (s, 3H, OCH_3), 3.61 (m, 4H, CH_2Cl and $C\underline{H}_2CH_2Cl$), 2.39 (t, 7.3 Hz, 2 H, NHC═$OC\underline{H}_2$), 2.27 (t, 7.3 Hz, 2H, $C\underline{H}_2COOCH_3$), 1.97 (qt, 7.3 Hz, 2H, $CH_2C\underline{H}_2CH_2$).

^{13}C NMR ($CDCl_3$, 125 MHz): $\delta = 173.4$ (C═ONH), 172.4 ($\underline{C}$═$OOCH_3$), 51.8 (OCH_3), 44.2 (CH_2Cl), 41.3 ($NHCH_2$), 35.5 (NHC═$O\underline{C}H_2$), 33.1 (CH_3C═$O\underline{C}H_2$), 20.9 ($CH_2\underline{C}H_2CH_2$).

ESI MS: *m/z*: calculated 207.07, found 208.0 and 210.0 [$M + H^+$].

Synthesis of 2-methoxycarbonylpropyl-2-oxazoline (2, C3MestOx)

The C3MestOx precursor (**2b**, 60 g, 289 mmol) and anhydrous sodium carbonate (27.6 g, 260 mmol) were mixed. The reaction was performed overnight by mounting the flask at the rotary evaporator (40 °C, 50 mbar) to allow good mixing of the salt in the viscous mixture and providing a larger surface area for evaporation of the released CO_2. Subsequently, DCM was added, the reaction mixture was filtered and the solvent was removed under reduced pressure. The oil was distilled twice over barium oxide, under reduced pressure, yielding a colorless liquid (24.8 g, 145 mmol, 50%).

^{1}H NMR ($CDCl_3$, 500 MHz): $\delta = 4.3$ (t, 2H, 9.5 Hz, CH_2O), 3.8 (t, 9.5 Hz, 2H, CH_2N═), 3.7 (s, 3H, $COOCH_3$), 2.7 (t, 2H, 7.3 Hz, CH_2COO), 2.6 (t, 2H, 7.3 Hz, CH_2C(═N)O)), 1.97 (quint, 7.3 Hz, 2H, $CH_2C\underline{H}_2CH_2$)

^{13}C NMR ($CDCl_3$, 75 MHz): $\delta = 173.6$ ($\underline{C}OOCH_3$), 167.8 (C(═N)O), 67.3 (CH_2O), 54.5 (CH_2N), 51.7 (OCH_3), 32.9 ($\underline{C}H_2COOCH_3$), 27.2 ($\underline{C}H_2C$(═N)O), 21.3 ($CH_2\underline{C}H_2CH_2$).

TABLE 1 Overview of Different Reaction Times at Different Temperatures Used for Kinetic Studies

Sample	140 °C All Monomers, Homo- and Copolymerization	120 °C MestOx and C3MestOx Homo, MeOx–MestOx	100 °C MestOx and C3MestOx Homo, MeOx–MestOx	80 °C MeOx, EtOx, *n*PropOx, MestOx Copolymerization	80 °C MestOx, C3MestOx, C3MestOx Copolymerization
1	1 s	1 s	7 min 30 s	20 min	35 min
2	2 min	7 min 30 s	15 min	40 min	70 min
3	4 min	15 min	30 min	60 min	105 min
4	6 min	22 min 30 s	45 min	80 min	140 min
5	8 min	30 min	1 h	100 min	175 min
6	10 min	37 min 30 s	1 h 15 min	120 min	210 min
7	12 min	45 min	1 h 30 min		245 min

ESI MS: m/z: calculated 171.09, found 172.1$[M + H^+]$.

HR-MS: m/z: theoretical 171.08954 Da, found 172.0976 Da $[M + H^+]$; Δ abundance 4.6 ppm.

Synthesis of 2-n-propyl-2-oxazoline (5, nPropOx)

nPropOx was synthesized according to literature.[34] In brief, butyronitrile (1 equiv.), amino ethanol (1.1 equiv.) and zinc acetate dihydrate (catalyst, 0.02 equiv.) were refluxed at 130 °C overnight. The reaction mixture was cooled to room temperature, and dichloromethane was added. The organic phase was washed three times with water and once with brine. After removing the dichloromethane under reduced pressure, the monomer was purified by fractional distillation over barium oxide.

Polymerization Kinetics

Stock solutions (7 mL) for polymerization kinetics were prepared in the glovebox. The total monomer concentration $[M_{tot}] = [M_1] + [M_2]$ is 3 M, the monomer $(M_1 + M_2)$:initiator ratio $\frac{[M]}{[I]} = 100$, MeOTs was used as an initiator, acetonitrile (CH_3CN) was used as solvent. For copolymerizations the molar ratio of both monomers was 50:50. The stock solution was divided in 0.7 mL portions in separate 0.5–2 mL Biotage reaction vials. The polymerization times used are listed in Table 1. After the polymerization, 0.1 mL of polymerization mixture was sampled and diluted with 0.9 mL of chloroform for GC measurement. Conversion was determined based on the integral of monomer peaks using CH_3CN as an internal standard. A second sample of 0.1 mL was diluted with 0.9 mL of DMA containing 50 mM of LiCl for SEC measurement to determine M_n and $Đ$.

Computational Methodology

A density functional theory (DFT) study was performed to rationalize the polymerization kinetics of 2-oxazolines.[28,35] The Gaussian 09 program package[36] and the M06-2X/6-31+G(d,p) level of theory[37] were used for all static calculations. The most stable conformations (minima) of the 2-oxazolines and their *N*-methyl oxazolinium cations were found by means of conformational scans. Transition states (first-order saddle points) were located for several propagation systems and connected with their prereactive and product complexes by following the intrinsic reaction coordinate (IRC).[38–40] The nature of the minima and first-order saddle points was verified by frequency calculations. Hirshfeld-I (HI) charges were calculated for all systems,[41,42] since this charge scheme has proven useful for the analysis of the CROP of 2-oxazolines[28,35] and is relatively robust with respect to conformational changes.[42] In order to understand the dynamic behavior of the interactions between the side chains and the cationic centre, molecular dynamics simulations were performed on a MestOx decamer with the CP2K program[43] within an NVT ensemble using the semiempirical PM6 method.

RESULTS AND DISCUSSION

Monomer Synthesis

The 2-(methyl ester functionalized) 2-oxazoline monomers, MestOx, and C3MestOx, were prepared from commercially available acid chlorides **1a** (Scheme 3) and **2a** through a reaction with 2-chloroethylamine hydrochloride in the presence of triethylamine yielding intermediate compounds **1b** and **2b**. The monomers (**1** and **2**) were obtained by ring closure of these intermediate compounds with a strong non-

S3

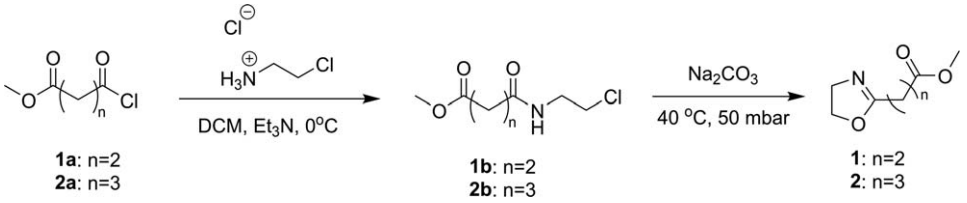

SCHEME 3 Synthesis of methyl ester containing 2-oxazolines.

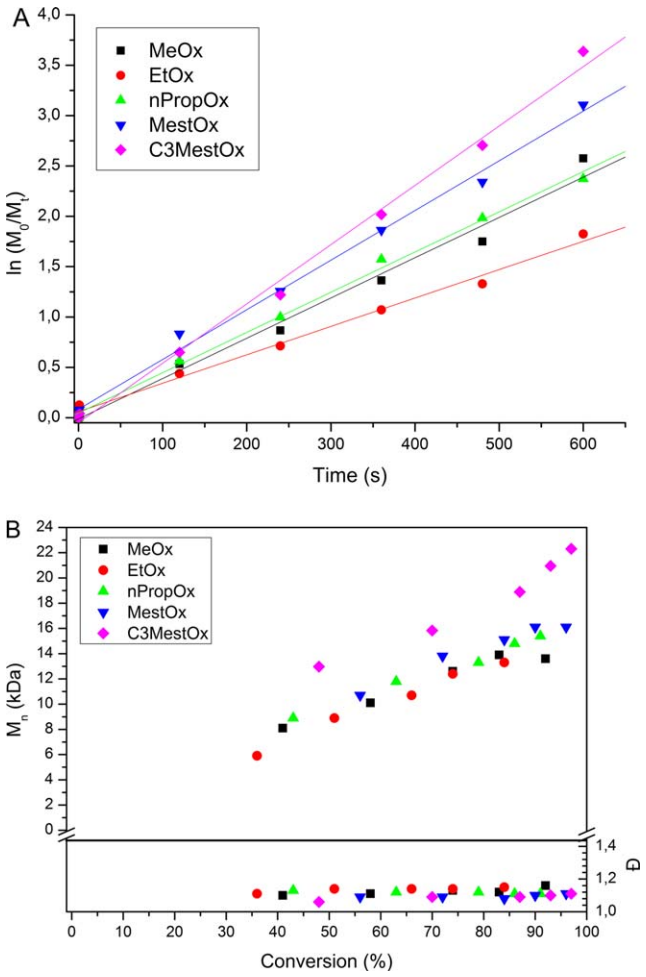

FIGURE 1 (A) First-order kinetic plot for homopolymerization of MeOx, EtOx, nPropOx, MestOx, and C3MestOx at 140 °C and (B) number average molecular weight (M_n) and dispersity ($Đ$) plotted against conversion. [Color figure can be viewed in the online issue, which is available at wileyonlinelibrary.com.]

nucleophilic base (sodium carbonate) to avoid saponification of the ester. This last reaction was performed on a rotary evaporator under reduced pressure to allow good mixing of the precursor oil and the salt and to ease the release of carbon dioxide.[28] The monomers were obtained pure and dry after distilling them twice over barium oxide. It should be noted that the synthesis of C3MestOx was easier due to the lower viscosity of the amide precursor **2b** in comparison to **1b**. As a result, the ring-closing reaction that involves release of CO_2 proceeded significantly faster.

Polymerization Kinetics

Homopolymerizations

All monomers (MestOx, C3MestOx, MeOx, EtOx, and nPropOx) were polymerized with methyl p-toluenesulfonate (MeOTs) as initiator,[44] acetonitrile as solvent under microwave irradiation at both 80 and 140 °C. Stock solutions were prepared which contained solvent, monomers and initiator at 3 M monomer concentration and a $[M]/[I]$ ratio of 100. The corresponding first order kinetic plots obtained at 140 °C reveal linear first-order kinetics for all monomers, indicating a constant concentration of propagating species in time and, thus, the absence of termination reactions albeit chain transfer can not be excluded [Fig. 1(A)]. Each data point represents a separate polymerization and, thus, the linearity of these combined results proves the good reproducibility. The livingness of the homopolymerizations was confirmed by a linear increase of the number average molecular weight (M_n) with conversion as well as the low dispersities of the resulting polymers ($Đ < 1.17$, 1B). Similar results were obtained at 80 °C, also revealing living polymerization of all monomers (Supporting Information Figs. S1 and S2).

The polymerization rate constants (k_p) were calculated from the slope of the linear correlation between $\ln([M]_0/[M]_t)$ and time in the first-order kinetic plots in Figure 1 and Supporting Information Figures S1 and are summarized in Table 2. The rates obtained for MeOx and EtOx are in good agreement with previously reported values,[34] but the k_p values of nPropOx at 140 °C is slightly higher due to a small overshoot in temperature to 150 °C during microwave heating of the polymerization mixture.

Previous computational work revealed that the fast propagation of the MestOx monomer is due to an interaction of the oxazolinium ring with the ester group in the side chain of the MestOx, leading to higher electrophilicity of the 5 position and thus enhancing the reactivity of the living chain end.[28] A similar intramolecular activation was proposed between the amide carbonyl of the last monomer before the oxazolinium chain end, leading to a higher k_p value compared to $k_{p,1}$ value for the first monomer addition during CROP.[33]

TABLE 2 Propagation Rate Constants for the Homopolymerizations

Monomer 1	T (°C)	k_p (10^{-3} L mol^{-1} s^{-1})	T (°C)	k_p (10^{-3} L mol^{-1} s^{-1})	T (°C)	k_p (10^{-3} L mol^{-1} s^{-1})	T (°C)	k_p (10^{-3} L mol^{-1} s^{-1})
MeOx	140	133 ± 4					80	4.13 ± 0.15
EtOx	140	99 ± 3					80	2.99 ± 0.05
nPropOx	140[a]	133 ± 4					80	3.86 ± 0.27
MestOx	140	171 ± 4	120	58.6 ± 2.2	100	28.0 ± 1.6	80	6.91 ± 0.29
C3MestOx	140	193 ± 4	120	48.6 ± 1.4	100	16.6 ± 0.8	80	5.29 ± 0.38

[a] Value is slightly higher due to a small overshoot in temperature to 150 °C during microwave heating of the polymerization mixture.

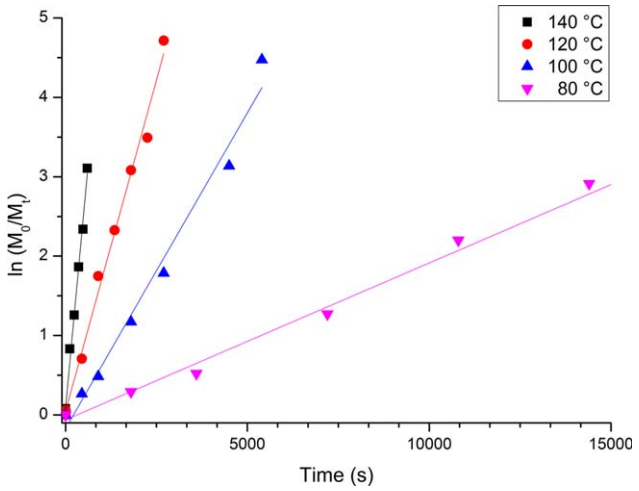

FIGURE 2 First-order kinetic plot for homopolymerization of MestOx at different temperatures. [Color figure can be viewed in the online issue, which is available at wileyonlinelibrary.com.]

At 140 °C C3MestOx is polymerizing faster than MestOx, while at 80 °C the order is reversed, but both of them are still faster than MeOx, EtOx, and nPropOx (Table 2). Similar results were obtained for the intermediate temperatures 120 and 100 °C, also revealing linear living polymerization kinetics (Fig. 2 and Supporting Information Figures S3–S5). At these temperatures MestOx also polymerizes faster than C3MestOx.

The logarithms of the k_p values of MestOx and C3MestOx show a linear relationship with the inverse temperature as expected based on the Arrhenius equation (eq 1).

$$k_p = Ae^{\frac{-E_A}{RT}} \quad (1)$$

The Arrhenius plots for the MestOx and C3MestOx homopolymerizations are shown in Figure 3. From these plots, the

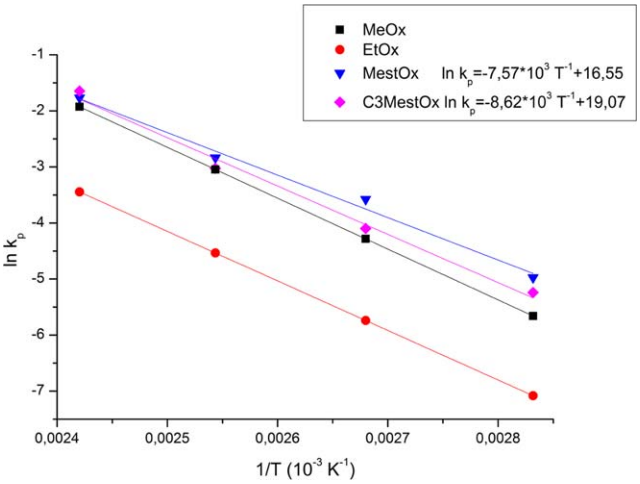

FIGURE 3 Arrhenius plot of MestOx and C3MestOx. The data from literature of MeOx[45] and EtOx[46] are included for comparison. [Color figure can be viewed in the online issue, which is available at wileyonlinelibrary.com.]

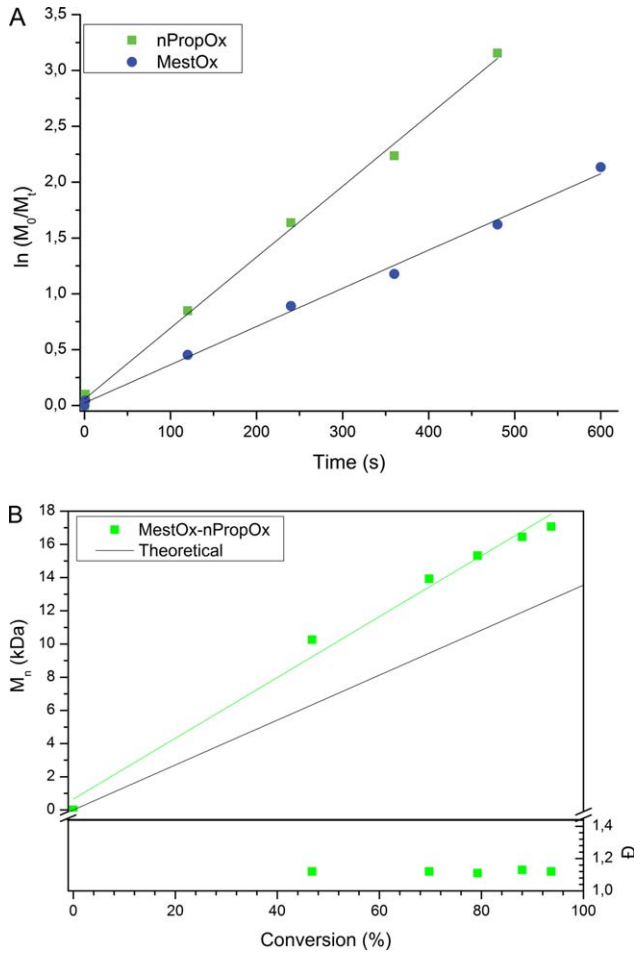

FIGURE 4 (A) First-order kinetic plot for copolymerization of nPropOx and MestOx at 140 °C and (B) number average molecular weight (M_n) and dispersity ($Đ$) plotted against conversion. [Color figure can be viewed in the online issue, which is available at wileyonlinelibrary.com.]

activation energy ($E_{A,\ MestOx} = 63.0 \pm 4.3$ kJ mol^{-1}, $E_{A,C3MestOx} = 71.7 \pm 4.9$ kJ mol^{-1}) and the frequency factor ($A_{MestOx} = 1.54 \pm 0.13 \times 10^7$ L mol^{-1} s^{-1}, $A_{C3MestOx} = 1.92 \pm 0.15 \times 10^8$ L mol^{-1} s^{-1}) were calculated. These activation energies are lower than for MeOx ($E_A = 75.4 \pm 0.5$ kJ mol^{-1})[45] and EtOx (73.4 ± 0.5 kJ mol^{-1}),[46] thereby indicating that the methyl ester groups indeed lower the activation barrier for monomer addition.

Copolymerizations

To further examine the remarkable copolymerization behavior of MestOx with MeOx and EtOx leading to reversed monomer incorporation order compared to the homopolymerization,[28] the copolymerization of MestOx and C3MestOx was studied with MeOx, EtOx, and nPropOx at both 80 and 140 °C with a monomer ratio of 50:50 using the same conditions as for the homopolymerizations. The previously reported copolymerizations of MestOx with MeOx or EtOx at 140 °C are also included to give a complete overview.[28]

TABLE 3 Propagation Rate Constants and Apparent Reactivity Ratios for the Copolymerizations of MestOx and C3MestOx with MeOx, EtOx, and nPropOx

Monomer 1	Monomer 2	T (°C)	$k_{p,1}$ (10^{-3} L mol^{-1} s^{1})	$k_{p,2}$ (10^{-3} L mol^{-1} s^{-1})	r_1^{app} (k_1/k_2)	r_2^{app} (k_2/k_1)
MeOx	MestOx	140	244 ± 6	89 ± 3	2.74	0.37
EtOx	MestOx	140	162 ± 4	97 ± 3	1.67	0.60
nPropOx	MestOx	140	212 ± 6	114 ± 3	1.86	0.54
MeOx	C3MestOx	140	184 ± 12	93 ± 8	1.98	0.50
EtOx	C3MestOx	140	144 ± 4	113 ± 3	1.26	0.79
nPropOx	C3MestOx	140	157 ± 7	109 ± 6	1.44	0.70
MeOx	MestOx	120	73.3 ± 6.3	27.1 ± 1.8	2.71	0.37
MeOx	MestOx	100	29.2 ± 1.4	8.90 ± 0.44	3.29	0.30
MeOx	MestOx	80	5.09 ± 0.13	1.34 ± 0.07	3.79	0.26
EtOx	MestOx	80	4.50 ± 0.26	2.68 ± 0.20	1.68	0.60
nPropOx	MestOx	80	4.65 ± 0.13	2.45 ± 0.16	1.90	0.53
MeOx	C3MestOx	80	7.91 ± 0.62	3.36 ± 0.03	2.36	0.42
EtOx	C3MestOx	80	5.80 ± 0.26	4.10 ± 0.14	1.41	0.71
nPropOx	C3MestOx	80	7.37 ± 0.38	5.27 ± 0.24	1.40	0.72

The first-order kinetic plots of nPropOx and MestOx copolymerization at 140 °C is shown in Figure 4(A) as representative example for all copolymerizations (Supporting Information Figs. S6–S27). For all investigated copolymerizations, the 2-alkyl-2-oxazoline monomer was incorporated faster than MestOx and C3MestOx in agreement with our previous findings.[28]

Modeling showed that the monomers bearing alkyl and methyl ester side chains compete for incorporation into the same living chain, which is activated due to the interaction between nearby MestOx and C3MestOx residues and the chain end. Since the reacting nitrogen atom is more negative and thus more nucleophilic in the monomers bearing alkyl side chains, these monomers are incorporated faster into the chain. The ester group in the growing polymer can also interact with the incoming MeOx monomer, inducing higher nucleophilicity of the MeOx monomer. The same interactions are expected to occur during (co)polymerization of C3MestOx.

All first-order kinetic plots revealed a linear increase, indicating a constant concentration of propagating species in time and, thus, the absence of termination reactions. Each data point represents a separate polymerization and, thus, the linearity proves the good reproducibility. The livingness of the polymerization was confirmed by the linearly increasing M_n with conversion as well as low dispersities ($Đ$) [Fig. 4(B)]. The discrepancy with the theoretical M_n values can be addressed to the PMMA standards, that is, the different hydrodynamic volume, used for the SEC calibration of the experimental values as shown previously.[28]

The k_p values were calculated from the slope of the kinetic plots and are summarized in Table 3. Compared to the k_p values of the homopolymerization, the incorporation of 2-alkyl-2-oxazoline monomers is accelerated while the incorporation of MestOx and C3MestOx is slowed down. This is due to the activation of the alkyl monomer by the interaction of the incoming alkyl monomer with the methyl ester side chain of the growing polymer chain.

By dividing both k_p values the apparent reactivity ratios (r^{app}) for both monomers are calculated (Table 3).[47] For copolymerizations of MestOx and C3MestOx with EtOx and nPropOx, changing the polymerization temperatures (140 and 80 °C) did not influence the r^{app} and, thus, the monomer distribution of the resulting polymer is independent of the temperature. In fact, for these copolymerizations r_1^{app} is less than 1.9 while r_2^{app} is larger than 0.5, so there is only a

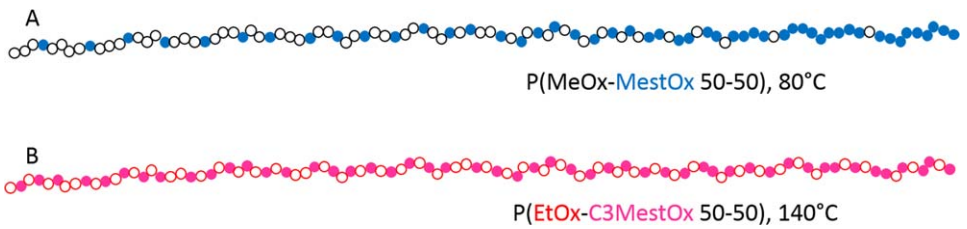

FIGURE 5 Monomer distribution of (A) MeOx (black, open) and MestOx (blue) after 80 °C copolymerization and (B) EtOx (red, open) and C3MestOx (pink) after copolymerization at 140 °C along the polymer chain, calculated from the kinetics plots. [Color figure can be viewed in the online issue, which is available at wileyonlinelibrary.com.]

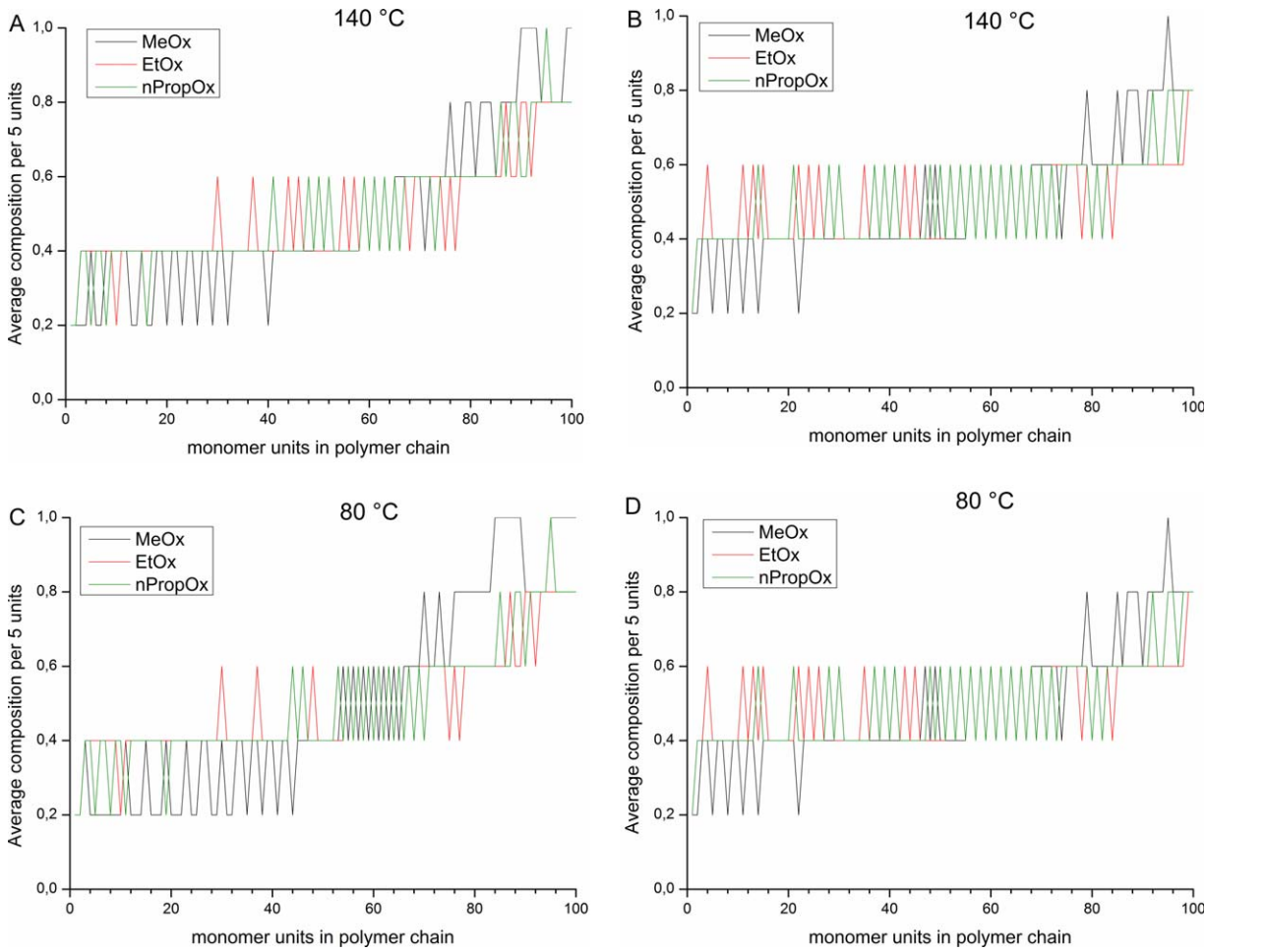

FIGURE 6 Gradient plots of the instantaneous copolymer composition along the polymer chains for (A) MestOx copolymers at 140 °C, (B) C3MestOx copolymers at 140 °C, (C) MestOx copolymers at 80 °C, and (D) C3MestOx copolymers at 80 °C. On the *y* axis 0 refers to no MestOx, 1 refers to fully MestOx and 0.5 to an equimolar mixture of both monomers. [Color figure can be viewed in the online issue, which is available at wileyonlinelibrary.com.]

minor deviation from an ideal random monomer distribution. The visualization of the monomer distributions in Figures 5(B) and 6 that are calculated based on the individual monomers conversions in time confirms a near ideal random structure for $r_1^{\text{app}} < 1.9$.

The copolymerizations of the more reactive MeOx with MestOx and C3MestOx have an r_1^{app} which is larger than 1.9 and a r_2^{app} is smaller than 0.5, so the monomer distribution significantly deviates from an ideal random distribution, for example, a gradient copolymer is formed. The strength of the gradient is determined by temperature and monomer. Lower temperatures lead to stronger gradients while copolymers with MestOx also have a stronger gradient than copolymers with C3MestOx.

From the first-order kinetic plots the average distribution of monomers along the polymer chain can be calculated. In Figure 5 two extremes are shown, in A the strongest gradient obtained from MeOx and MestOx copolymerized at 80 °C and in B the near random distribution of EtOx and C3MestOx

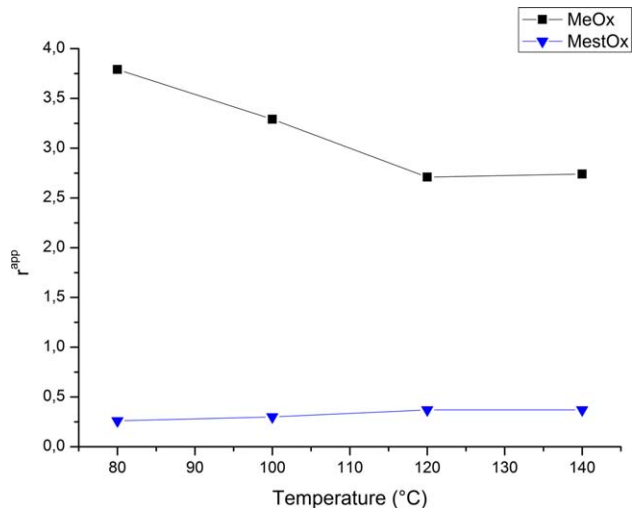

FIGURE 7 Temperature dependence of the apparent reactivity ratios of MeOx–MestOx copolymerization. [Color figure can be viewed in the online issue, which is available at wileyonlinelibrary.com.]

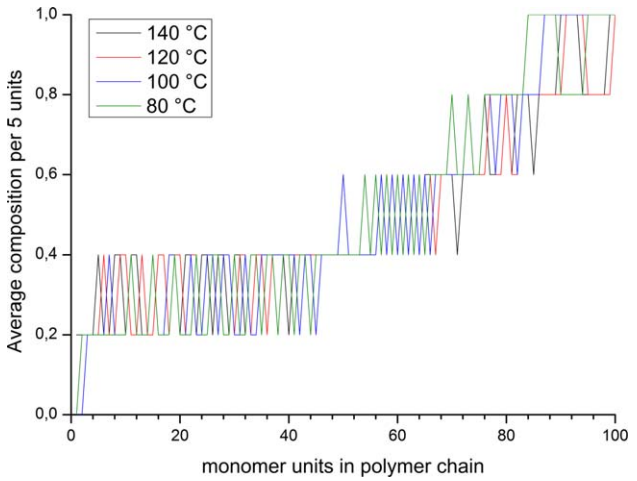

FIGURE 8 Gradient plots of MeOx–MestOx copolymerization at different temperatures. On the *y* axis 0 refers to no MestOx, 1 refers to fully MestOx, and 0.5 to an equimolar mixture of both monomers. [Color figure can be viewed in the online issue, which is available at wileyonlinelibrary.com.]

copolymerized at 140 °C. For easier comparison the different gradients are also plotted in Figure 6 clearly showing that the first part of the polymers is slightly enriched in the comonomer and the final part of the copolymer is enriched in (C3)MestOx.

As the MeOx–MestOx copolymerization showed the strongest gradient formations as well as a temperature dependence of the apparent reactivity ratios, the MeOx–MestOx kinetic studies were also performed at two intermediate temperatures (100 and 120 °C). Both temperatures also revealed linear first-order kinetics (Supporting Information Figs. S28 and S30), indicating a constant concentration of propagating species in time and, thus, absence of termination reactions. The livingness was confirmed by a linear increase of the M_n with conversion as well as $Đ$ values of the resulting polymer ($Đ < 1.13$, Supporting Information Figs. S29 and S31). The k_p values and r^{app} values are listed in Table 3. The apparent reactivity ratios are plotted ver-

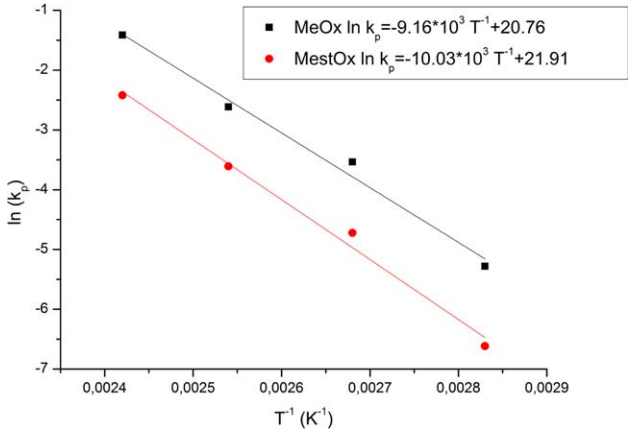

FIGURE 9 Arrhenius plot for the MeOx–MestOx copolymerization. [Color figure can be viewed in the online issue, which is available at wileyonlinelibrary.com.]

sus temperature in Figure 7, showing the temperature dependence of the apparent reactivity ratios between 80 and 120 °C while increasing further to 140 °C has no effect. The gradient plots of MeOx–MestOx copolymerizations at different temperatures are depicted in Figure 8, showing slightly stronger gradient formation at lower temperatures. Because the k_p values were determined at different temperatures, an Arrhenius plot could be made (Fig. 9) and from this the activation energy ($E_{A,\ MeOx} = 76.1 \pm 5.8$ kJ mol^{-1}, $E_{A,MestOx} = 83.4 \pm 5.6$ kJ mol^{-1}), and the frequency factor ($A_{MeOx} = 1.04 \pm 0.09 \times 10^7$ L mol^{-1} s^{-1}, $A_{MestOx} = 3.27 \pm 0.27 \times 10^9$ L mol^{-1} s^{-1}) were calculated. The activation energy of MeOx in the copolymerization is a comparable to the activation energy of MeOx in homopolymerization ($E_{A,MeOx} = 75.4$ kJ mol^{-1}), while the activation of the MestOx raised in comparison with homopolymerization ($E_{A,\ MestOx} = 63.0 \pm 4.3$ kJ mol^{-1}).

Computational Rationalization

In order to rationalize the difference in polymerization kinetics between 2-oxazolines bearing aliphatic (MeOx, EtOx, nPropOx) and methyl ester side chains (MestOx, C3MestOx), at first, a density functional theory (DFT) study was performed.[28,35] 2-oxazolines and their *N*-methyl-2-oxazolinium cations were studied as model systems for monomers and living chain ends, respectively. Subsequently, a dimeric living end was used to model the second propagation step for several systems. As a final step, a molecular dynamics simulation of a model polymer—MestOx decamer—was performed to investigate the dynamic behavior of the polymer chain and the time evolution of interactions within the living chain.

Various conformers were localized for the isolated oxazoline monomers and their *N*-methyl oxazolinium cations corresponding to different orientations of the side chain with respect to the five-membered ring. The relative free energies of these conformations are listed in Table 4, alongside Hirshfeld-I charges of the N3 and C5′ ring atoms. These charges will be used as measures for the nucleophilicity of the monomer and the electrophilicity of the living chain, respectively. The Hirshfeld-I charge scheme has been successfully used to rationalize k_p's for the CROP of 2-oxazoline polymerizations[28,35] and is robust with respect to conformational changes.[42]

The extended (ext) and interacting (int) conformations of MestOx, C3MestOx (Fig. 10) and nPropOx systems stem from the bond rotations in the side chain, since the five-membered oxazoline and oxazolinium rings are relatively rigid. MestOx and C3MestOx cations preferentially adopt a contracted or interacting conformation in which the side chain interacts with the oxazoline ring ($\Delta G_{int-ext}$(MestOx) $= -33.5$ kJ mol^{-1}, $\Delta G_{int-ext}$ (C3MestOx) $= -27.4$ kJ mol^{-1}). This electrostatic cation–dipole interaction between the oxazolinium ion and the carbonyl group of the MestOx side chain is an important factor in the k_p increase of MestOx and C3MestOx and can be found in prereactive complexes of propagations and molecular dynamics simulations of longer living chains (see further).

TABLE 4 Relative Gibbs-Free Energy and N3/C5′ Hirshfeld-I Charges of the Most Stable Monomer and Cation Conformations (ext = extended, int = interacting, M06-2X/6–31+G(d,p), 413.15 K, 1 atm)

		Monomer		Cation	
		ΔG (kJ mol^{-1})	N3 (e)	ΔG (kJ mol^{-1})	C5′ (e)
MeOx			−0.578		0.041
EtOx			−0.582		0.040
NPropOx	ext	0.0	−0.581	0.0	0.044
	int	4.0	−0.586	0.1	0.045
MestOx	ext	0.0	−0.567	0.0	0.040
	int	12.6	−0.577	−33.5	0.047
C3MestOx	ext	0.0	−0.568	0.0	0.040
	int	5.2	−0.570	−27.4	0.057

The opposite is true for the monomers: extended side chains are favored over interacting conformations in these cases ($\Delta G_{\text{int–ext}}$ (MestOx) = 12.6 kJ mol^{-1}, $\Delta G_{\text{int–ext}}$ (C3MestOx) = 5.2 kJ mol^{-1}, $\Delta G_{\text{int–ext}}$ (nPropOx) = 4.0 kJ mol^{-1}). The conformers are equally stable in the case of nPropOx cations ($\Delta G_{\text{int–ext}}$ (nPropOx) = 0.1 kJ mol^{-1}).

The charge of the 2-oxazoline nitrogen atom N3 is a measure for the nucleophilicity of the monomer. Therefore, 2-oxazolines with aliphatic side chains (MeOx −0.578, EtOx −0.582, nPropOx −0.581) are more nucleophilic than those with methyl ester side chains (MestOx −0.577, C3MestOx −0.570). The lower nucleophilicity of the methyl ester containing monomers can be ascribed to a reduction of the electron donating character of the aliphatic side chains resulting from the electron withdrawing nature of the methyl ester group. This leads to the observed incorporation rate in copolymerizations: if both types of monomers compete for addition to the same living chain end, the aliphatic monomers are more likely to react. The charge of the oxazolinium carbon atom C5′ is a measure for the electrophilicity of the living homopolymer chain end. Cations with aliphatic side chains are less electrophilic (MeOx 0.041, EtOx 0.040, nPropOx 0.044) than those with methyl

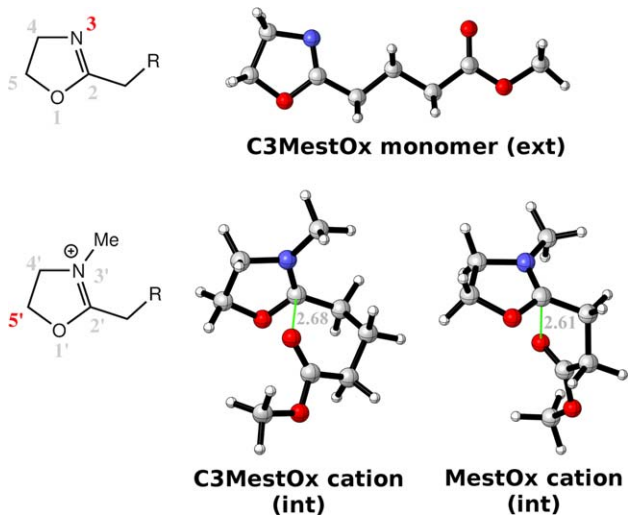

FIGURE 10 Most stable conformation of the C3MestOx monomer and C3MestOx and MestOx cation (ext = extended, int = interacting, M062X/6–31+G(d,p)). [Color figure can be viewed in the online issue, which is available at wileyonlinelibrary.com.]

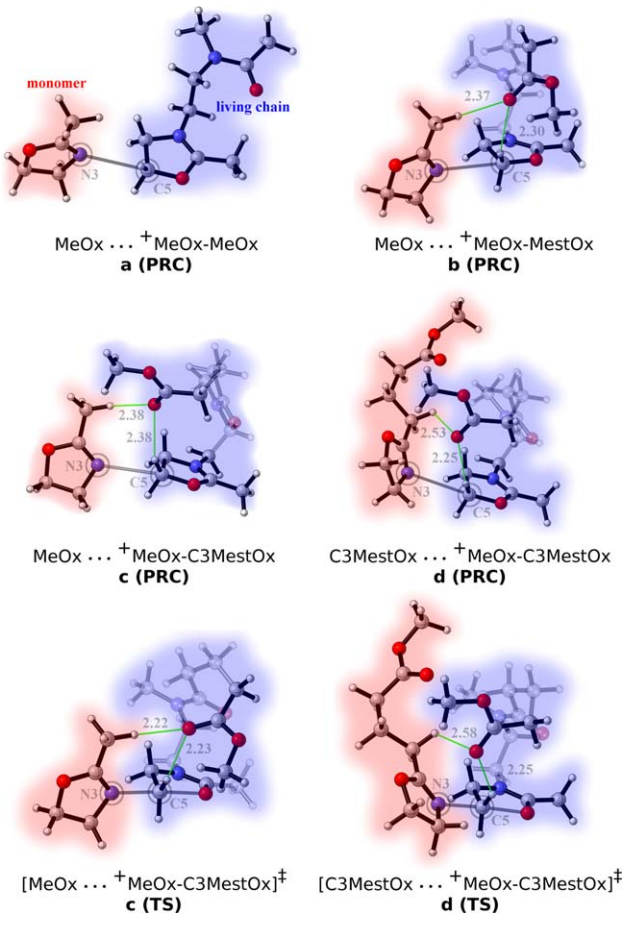

FIGURE 11 Geometries of selected pre-reactive complexes and transition states (distances in Å, interactions in green, monomers in red living chains in blue, M06-2X/6–31+G(d,p), propagation systems **a–f** in Table 5). [Color figure can be viewed in the online issue, which is available at wileyonlinelibrary.com.]

TABLE 5 N3/C5′ Hirshfeld-I Charges of Selected Prereactive Complexes (M06-2X/6–31+G(d,p), 413.15 K, 1 atm)

	Monomer	Living Chain	N3 (e)	C5′ (e)
A	MeOx	$^{+}$MeOx–MeOx	−0.635	0.065
b	MeOx	$^{+}$MeOx–MestOx	−0.623	0.070
C	MeOx	$^{+}$MeOx–C3MestOx	−0.631	0.074
D	C3MestOx	$^{+}$MeOx–C3MestOx	−0.610	0.071

ester side chains (MestOx 0.047, C3MestOx 0.057), given the methyl ester interacts with the ring (MestOx: 0.047 vs. 0.040, C3MestOx: 0.057 vs. 0.040). The longer C3MestOx side chain (trimethylene spacer) causes a larger electrophilicity increase than the shorter MestOx side chain (ethylene spacer). This electrophilicity increase is almost absent in nPropOx (nPropOx: 0.045 vs. 0.044). Due to steric/torsional effects, the MestOx side chain is positioned closer to the cationic center (2.61 Å, Fig. 11) than the C3MestOx side chain (2.68 Å).

As a consequence, two opposing effects come into play during the homopolymerization of 2-oxazolines bearing methyl ester side chains: less nucleophilic monomers and more electrophilic living chain ends. For 2-oxazolines bearing aliphatic side chains, the situation is reversed: more nucleophilic monomers, but less electrophilic living chain ends. Since the same order (C3MestOx > MestOx > nPropOx > MeOx > EtOx) was found for C5′ charges (0.057 > 0.047 > 0.045 > 0.041 > 0.040) and homopolymerization rates (Table 2, $k_p(10^{-3}$ L mol^{-1} s) at 140 °C: 192.7 > 171.0, 133.2 > 132.7 > 98.7), the electrophilic effect is seemingly more important for these 2-oxazolines. MestOx and C3MestOx homopolymerizations are faster due to the interaction between the methyl ester side chain and the 2-oxazolinium ring.

The rate-enhancing effect of methyl ester side chains is not limited to single-unit chains, such as the *N*-methyl oxazolinium cations, since nearby MestOx and C3MestOx residues can contribute to the electrophilicity and nucleophilicity increase as well. In order to obtain a deeper insight into the role of the nearby side chains, four propagation reactions **a–d**, in which a monomer is incorporated into a dimeric living chain, were studied (Table 5 and Fig. 11) and a molecular dynamics simulation was performed on a MestOx decameric living chain (Fig. 12).

The nearby MestOx and C3MestOx residues in the prereactive complexes of propagation reactions **b–d** coordinate toward the reactive center. The carbonyl oxygen atom of their methyl ester side chain interacts with one of the hydrogen atoms attached to the electrophilic carbon atom C5′ (**b**: 2.30 Å, **c**: 2.38 Å, **d**: 2.25 Å). This interaction withdraws electron density from the cationic ring, thereby increasing the electrophilicity of the living chain end (Table 5, see further). Since there is no methyl ester side chain present in the MeOx homopolymerization (**a**), the corresponding living chain end is less electrophilic.

The carbonyl oxygen of the methyl esters interacts with the chain end through one of the hydrogens atoms attached to C5′ and with one of the hydrogen atoms attached to the first methyl(ene) group of the monomer side chain, both in the transition states (SI) and the prereactive complexes of these propagations (Fig. 11).

In the prereactive complexes of these larger systems [Fig. 11(a–d), Hirshfeld-I charges in Table 5], the reactive nitrogen atom N3 is more nucleophilic ($-0.635 \leq N3 \leq -0.610$ in PRCs, $-0.586 \leq N3 \leq -0.567$ in isolated monomers) and the reactive carbon atom more electrophilic ($0.065 \leq C5' \leq 0.074$ in PRCs, $0.040 \leq C5' \leq 0.057$ in isolated cations) than in the isolated monomers and cations, respectively. Complexation of the reactants thus increases the reactivity, regardless of the nature of the side chain. The higher nucleophilicity of the MeOx monomer is confirmed ($-0.635 \leq N3 \leq -0.623$ for MeOx, −0.610 for C3MestOx). If nearby methyl esters are present in the living dimer (**b–d**), the electrophilicity of the living chain is increased relative to the MeOx homopolymerization **a** (0.065 for **a**, $0.070 \leq C5' \leq 0.074$ for **b–d**). This electrophilicity increase is larger for C3MestOx (0.074 for **c**) than for MestOx (0.070 for

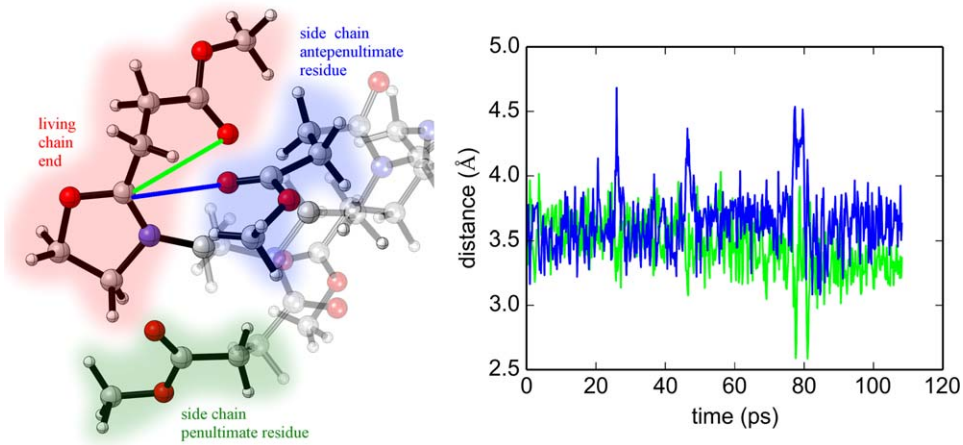

FIGURE 12 Snapshot of a MestOx homodecamer and selected distances during an MD simulation (selected interactions as green and blue lines, PM6, NVT at 300 K). [Color figure can be viewed in the online issue, which is available at wileyonlinelibrary.com.]

b), in accordance with the charges of *N*-methyl 2-oxazolinium cations.

The conformational space of the methyl ester groups and their interactions with the oxazolinium chain end were investigated by means of a semiempirical molecular dynamics (MD) simulation of an elongated living chain (Fig. 12). A trajectory of about 100 ps was obtained for a cationic MestOx homodecamer. Herein, two important interactions can be discerned: (a) one between the oxazolinium ring and the side chain of the terminal residue (green line) and (b) one between the side chain of the antepenultimate residue ($^{+}$MestOx–MestOx–**MestOx**–MestOx$_7$) and the ring (blue line). Remarkably, the side chain of the penultimate residue ($^{+}$MestOx–**MestOx**–MestOx–MestOx$_7$) is positioned further away from the ring (≈5 Å) than that of the antepenultimate residue (≈3.5 Å). Irrespective of their position in the living chain, methyl ester groups can cause intrachain stabilization by coordinating toward the chain end when sterically allowed. Similar behavior may also lead to interchain stabilization when multiple living chains are in contact.

The calculations on isolated reactants and extended systems are in good correlation. Interactions between the methyl ester groups of the reactive or nearby residues and the chain end withdraw electron density from the reactive carbon atom and render the living chain more electrophilic. This explains the higher homopolymerization rate of MestOx and C3MestOx. Similar rate increases are found in the copolymerizations of MeOx/EtOx/nPropOx with MestOx/C3MestOx. In these reactions, different monomers compete for the same chain end and the nucleophilicity of each monomer controls its rate of incorporation.

CONCLUSIONS

The methyl ester containing 2-oxazoline monomers, MestOx and C3MestOx, were successfully synthesized via the reaction of an acid chloride with 2-chloroethylamine and subsequent ring closure with sodium carbonate. Homopolymerization kinetic studies revealed a faster propagation of MestOx and C3MestOx compared to the alkyl monomers, MeOx, EtOx, and *n*PropOx, while in copolymerization a reversal of monomer incorporation was found, yielding a gradual change of monomer composition along the polymer from MeOx, EtOx, or nPropOx to MestOx or C3MestOx. EtOx and nPropOx copolymerizations lead to a minor deviation from ideal random monomer distribution, while copolymerization with MeOx leads to temperature-dependent gradient formation.

A theoretical rationalization shows that methyl ester groups in MestOx and C3MestOx living chains interact with the living chain end, thereby increasing its electrophilicity. This interaction was found in static DFT calculations on *N*-methyl 2-oxazolinium cations, as well as in a molecular dynamics simulation of a MestOx decameric living chain. Both methyl ester groups attached to the terminal residue and to nearby residues can interact with the oxazolinium chain end. However, the nucleophilicity of 2-oxazolines bearing alkyl side chains (MeOx, EtOx, and nPropOx) is larger than that of MestOx and C3MestOx. The electrophilicity increases were shown to be more important in determining the rate of propagation than the inherent monomer nucleophilicity. This explains the faster homopolymerization of MestOx and C3MestOx. In copolymerizations, however, multiple monomers compete for the same living chain end and the most nucleophilic one will be incorporated faster. This was confirmed by modeling the incorporation of a monomer into a dimeric living chain for several polymerization systems.

ACKNOWLEDGMENTS

The computational resources used in this work were provided by Stevin Supercomputer Infrastructure Ghent University (Belgium), the Hercules Foundation, and the Flemish Government—Department EWI. V.V.S. and R.H. acknowledge the Belgian Program on Interuniversity Attraction Poles initiated by the Belgian State, the Prime Minister's office (P7/05) and the IWT for support via the Strategic Basic Research program (SBO-120049). P.B and J.v.H. acknowledge the Polymer Innovation Program (PIPM10006, General adhesive Tissue Tape). All authors acknowledge the Special Research Fund of Ghent University; in particular PB for a joint PhD fellowship.

REFERENCES AND NOTES

1 W. Seeliger, E. Aufderhaar, W. Diepers, R. Feinauer, R. Nehring, W. Thier, H. Hellmann, *Angew. Chem. Int. Ed.* **1966**, *5*, 875–888.

2 D. A. Tomalia, D. P. Sheetz, *J. Polym. Sci., Part A: Polym. Chem.* **1966**, *4*, 2253–2265.

3 T. Kagiya, S. Narisawa, T. Maeda, K. Fukui, *J. Polym. Sci. Polym. Lett.* **1966**, *4*, 441–445.

4 T. G. Bassiri, A. Levy, M. Litt, *J. Polym. Sci., Part B: Polym. Lett.* **1967**, *5*, 871–879.

5 M. W. M. Fijten, C. Haensch, B. M. van Lankvelt, R. Hoogenboom, U. S. Schubert, *Macromol. Chem. Phys.* **2008**, *209*, 1887–1895.

6 R. Hoogenboom, *Angew. Chem. Int. Ed.* **2009**, *48*, 7978–7994.

7 G. Volet, T. X. Lav, J. Babinot, C. Amiel, *Macromol. Chem. Phys.* **2011**, *212*, 118–124.

8 B. Guillerm, S. Monge, V. Lapinte, J. J. Robin, *Macromol. Rapid Commun.* **2012**, *33*, 1600–1612.

9 V. Schenk, E. Rossegger, C. Ebner, F. Bangerl, K. Reichmann, B. Hoffmann, M. Höpfner, F. Wiesbrock, *Polymers* **2014**, *6*, 264–279.

10 S. Zalipsky, C. B. Hansen, J. M. Oaks, T. M. Allen, *J. Pharm. Sci.* **1996**, *85*, 133–137.

11 A. Mero, G. Pasut, L. D. Via, M. W. M. Fijten, U. S. Schubert, R. Hoogenboom, F. M. Veronese, *J. Control. Release* **2008**, *125*, 87–95.

12 R. Luxenhofer, Y. Han, A. Schulz, J. Tong, Z. He, A. V. Kabanov, R. Jordan, *Macromol. Rapid Commun.* **2012**, *33*, 1613–1631.

13 R. Luxenhofer, G. Sahay, A. Schulz, D. Alakhova, T. K. Bronich, R. Jordan, A. V. Kabanov, *J. Control. Release* **2011**, *153*, 73–82.

14 C. Diehl, H. Schlaad, *Macromol. Biosci.* **2009**, *9*, 157–161.

15 C. Weber, R. Hoogenboom, U. S. Schubert, *Prog. Polym. Sci.* **2012**, *37*, 686–714.

16 R. Hoogenboom, H. M. L. Thijs, M. J. H. C. Jochems, B. M. van Lankvelt, M. W. M. Fijten, U. S. Schubert, *Chem. Commun.* **2008**, *44*, 5758–5760.

17 A. Levy, M. Litt, *J. Polym. Sci., Part A: Polym. Chem.* **1968**, *6*, 1883–1894.

18 M. T. Zarka, O. Nuyken, R. Weberskirch, *Chem. Eur. J.* **2003**, *9*, 3228–3234.

19 T. Kotre, M. T. Zarka, J. O. Krause, M. R. Buchmeiser, R. Weberskirch, O. Nuyken, *Macromol. Symp.* **2004**, *217*, 203–214.

20 J. C. Rueda, S. Zschoche, H. Komber, F. Krahl, K. F. Arndt, B. Voit, *Macromol. Chem. Phys.* **2010**, *211*, 706–716.

21 Y. Liu, Y. Wang, Y. F. Wang, J. Lu, V. Pinon, M. Weck, *J. Am. Chem. Soc.* **2011**, *133*, 14260–14263.

22 S. Zschoche, J. C. Rueda, M. Binner, H. Komber, A. Janke, K. F. Arndt, S. Lehmann, B. Voit, *Macromol. Chem. Phys.* **2012**, *213*, 215–226.

23 J. C. Rueda, E. Campos, H. Komber, S. Zschoche, L. Haussler, B. Voit, *Des. Monom. Polym.* **2014**, *17*, 208–216.

24 C. Taubmann, R. Luxenhofer, S. Cesana, R. Jordan, *Macromol. Biosci.* **2005**, *5*, 603–612.

25 A. Gress, A. Volkel, H. Schlaad, *Macromolecules* **2007**, *40*, 7928–7933.

26 S. Zschoche, J. Rueda, V. Boyko, F. Krahl, K. F. Arndt, B. Voit, *Macromol. Chem. Phys.* **2010**, *211*, 1035–1042.

27 A. M. Kelly, A. Hecke, B. Wirnsberger, F. Wiesbrock, *Macromol. Rapid Commun.* **2011**, *32*, 1815–1819.

28 P. J. M. Bouten, D. Hertsen, M. Vergaelen, B. D. Monnery, M. A. Boerman, H. Goossens, S. Catak, J. C. M. van Hest, V. Van Speybroeck, R. Hoogenboom, *Polym. Chem.* **2015**, *6*, 514–518.

29 C. Legros, M.-C. D. Pauw-Gillet, K. C. Tam, S. Lecommandoux, D. Taton, *Eur. Polym. J.* **2015**, *62*, 322–330.

30 K. Lava, B. Verbraeken, R. Hoogenboom, *Eur. Polym. J.* **2015**, *65*, 98–111.

31 M. Mees, R. Hoogenboom, *Macromolecules*, **2015**, *48*, 3531–3538.

32 P. Steunenberg, P. M. Könst, E. L. Scott, Franssen, M. C. R.; Zuilhof, H.; Sanders, J. P. M. *Eur. Polym. J.* **2013**, *49*, 1773–1781.

33 T. Saegusa, H. Ikeda, *Macromolecules* **1973**, *6*, 808–811.

34 R. Hoogenboom, M. W. M. Fijten, H. M. L. Thijs, B. M. Van Lankvelt, U. S. Schubert, *Des. Monomers Polym.* **2005**, *8*, 659–671.

35 H. Goossens, S. Catak, M. Glassner, V. R. de la Rosa, B. D. Monnery, F. De Proft, V. Van Speybroeck, R. Hoogenboom, *ACS Macro Lett.* **2013**, *2*, 651–654.

36 M. Frisch, G. Trucks, H. Schlegel, G. Scuseria, M. Robb, J. Cheeseman, G. Scalmani, V. Barone, B. Mennucci, G. Petersson, Gaussian, Inc., Wallingford, CT, **2010**.

37 Y. Zhao, D. G. Truhlar, *Theor. Chem. Acc.* **2008**, *120*, 215–241.

38 K. Fukui, *Acc. Chem. Res.* **1981**, *14*, 363.

39 H. P. Hratchian, H. B. Schlegel, *J. Chem. Phys.* **2004**, *120*, 9918.

40 H. Hratchian, H. Schlegel, *J. Chem. Theory Comput.* **2005**, *1*, 61–69.

41 T. Verstraelen, V. Van Speybroeck, M. Waroquier, *J. Chem. Phys.* **2009**, *131*, 044127.

42 S. Catak, M. D'hooghe, T. Verstraelen, K. Hemelsoet, A. Van Nieuwenhove, H. J. Ha, M. Waroquier, N. De Kimpe, V. Van Speybroeck, *J. Org. Chem.* **2010**, *75*, 4530–4541.

43 Available at: http://cp2k.org/ Accessed 02 June **2015**.

44 M. Glassner, D. R. D'hooge, J. Young Park, P. H. M. Van Steenberge, B. D. Monnery, M.-F. Reyniers, R. Hoogenboom, *Eur. Polym. J.* **2015**, *65*, 298–304.

45 F. Wiesbrock, R. Hoogenboom, M. A. M. Leenen, M. A. R. Meier, U. S. Schubert, *Macromolecules* **2005**, *38*, 5025–5034.

46 F. Wiesbrock, R. Hoogenboom, C. H. Abeln, U. S. Schubert, *Macromol. Rapid Commun.* **2004**, *25*, 1895–1899.

47 J. E. Puskas, K. B. McAuley, S. W. P. Chan, *Macromol. Symp.* **2006**, *243*, 46–52.